Geochronology, Petrology, and Genesis of Two Granitic Plutons of the Xianghualing Ore Field in South Hunan Province: Constraints from Zircon U–Pb Dating, Geochemistry, and Lu–Hf Isotopic Compositions

Lizhi Yang [1], Xiangbin Wu [1,*], Jingya Cao [2,*] , Bin Hu [1], Xiaowen Zhang [3], Yushuang Gong [4] and Weidong Liu [5]

[1] Key Laboratory of Metallogenic Prediction of Nonferrous Metals and Geological Environment Monitoring, Ministry of Education, Central South University, No. 932, Lushan Road, Changsha 410083, China; yanglizhidz@csu.edu.cn (L.Y.); binhu1999@hotmail.com (B.H.)

[2] CAS Key Laboratory of Crust-Mantle Materials and Environments, University of Science and Technology of China, Hefei 230026, China

[3] School of Environment and Safety Engineering, University of South China, Hengyang 421001, China; zhangxiaowen02@sina.com

[4] Sinomine Resource Exploration Co. Ltd., Beijing 100089, China; gys1016@163.com

[5] No. 7 Institute of Geology and Mineral Exploration of Shandong Province, Linyi 276006, China; wolf1210@sina.com

* Correspondence: Wuxb133@126.com (X.W.); jingyacao@csu.edu.cn (J.C.)

Abstract: Two small-sized granitic plutons, outcropped in Xianghualing ore field, South Hunan (South China), have a close relationship with the super large-scale Sn–W polymetallic mineralization in this ore field. The Laiziling and Jianfengling plutons are composed of medium- to coarse-grained two-mica and coarse-grained biotite granites, respectively, and have zircon U–Pb ages of 156.4 ± 1.4 Ma and 165.2 ± 1.4 Ma, respectively. Both of the Laiziling and Jianfengling granites are characterized by extremely similar elemental and Lu–Hf isotopic compositions with high contents of SiO_2, Al_2O_3, Na_2O, K_2O, high A/CNK ratios, negative $\varepsilon_{Hf}(t)$ values (ranging from -3.86 to -1.38 and from -5.44 to -3.71, respectively), and old T_{DMC} ages (ranging from 1.30 to 1.47 Ga and from 1.32 to 1.56 Ga, respectively). These features indicate that they both belong to highly fractionated A-type granites, and were formed in an extensional setting and from the same magma chamber originated from the Paleoproterozoic metamorphic basement of South China with a certain amount of mantle-derived magma involved with temperatures of ca. 730 °C and low oxygen fugacity.

1. Introduction

South Hunan, located in the central part of the Shi-Hang zone, is well-known for its world-class W–Sn–Pb–Zn polymetallic deposits and reserves (Figure 1a). The Shi-Hang zone, well-known as the collision suture between the Yangtze Block and Cathaysia Block in the Neoproterozoic, is also an important granitic magmatic belt and polymetallic metallogenic belt [1–3]. As a significant part of the Shi-Hang zone, the W–Sn–Pb–Zn mineralization in this South Hunan possesses an obvious zoning feature from east to west: Shizhuyuan and Yaogangxian W deposits in the eastern part, Furong, Xianghualing and Furong Sn deposits in the middle part, and Huangshaping and Baoshan Pb–Zn

deposits in the western part (Figure 1b). Previous studies have revealed that these deposits were formed in 165–150 Ma, which were the significant part of the Jurassic metallogenic explosion event of South China [4–10]. In addition, these deposits have a genetic relationship with the granitic magmatic activity in this area, and it has been proved by the geological and geochronological evidences [4–9,11–15]. Due to the large-scale W–Sn–Pb–Zn polymetallic mineralization, the granitic plutons related with these large deposits have been drawn the attention of geologists, and abundant geochronological and geochemical data have been reported recently, such as Qitianling pluton (155.5 ± 1.3 Ma, associated with the Furong Sn deposit [13]), Qianlishan pluton (157 ± 2 Ma, associated with the Shizhuyuan W deposit [15]), Yaogangxian pluton (156.9 ± 0.7 Ma, associated with the Yaogangxian W deposit [11]), Huangshaping pluton (154.3 ± 1.9 Ma, associated with the Huangshaping Pb–Zn deposit [16]), and Baoshan pluton (158 ± 2 Ma, associated with the Baoshan Cu–Mo–Pb–Zn deposit [6]). These coeval granitic plutons in South Hunan, related to different metallic mineralization, have been an ideal place to probe into the magmatism and related mineralization of South China.
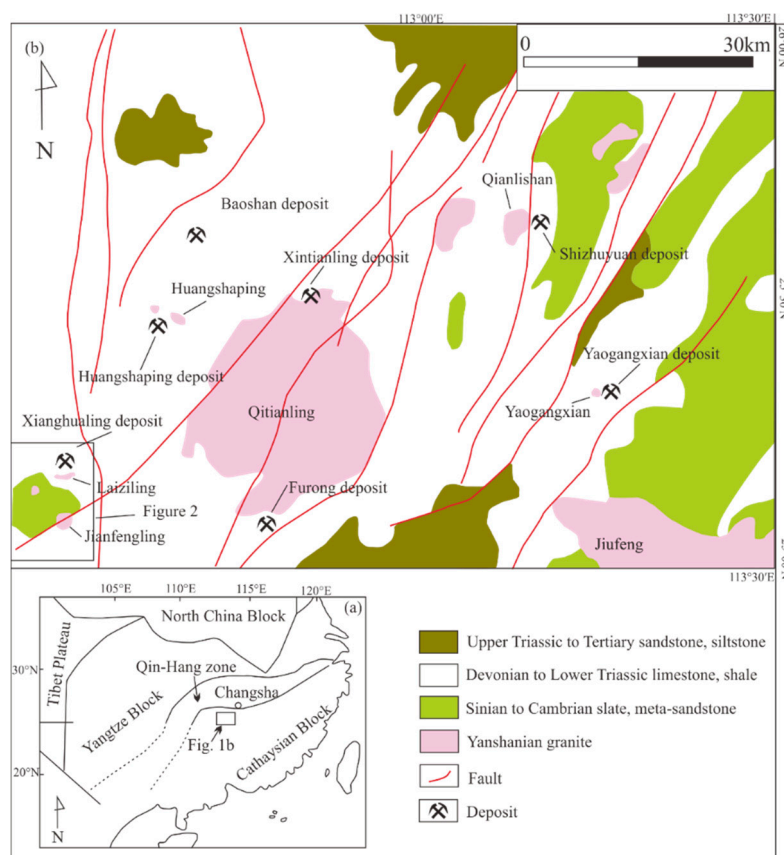
Figure 1. (**a**) Geological sketch map of South China; (**b**) Geological sketch map of the South Hunan province (modified from [8]), showing the distribution of granitic plutons, and related deposits.

The Laiziling and Jianfengling plutons, located in Xianghualing ore field, South Hunan province, are two small-sized granitic plutons, however, they have close relationship with the super-large Xianghualing Sn deposit and large Dongshan W deposit, respectively, both in time and space [7,17,18]. Then, it is the perfect laboratory for studying the theory of little intrusion forming large deposit. However, former studies have been focused on the abundant Sn–W polymetallic mineralization and genesis of the singly pluton. Additionally, a lack of systematic geochronological, geochemical, and isotopic analysis makes it unclear for the genesis and tectonic setting of these granitic plutons. Furthermore, few works have been conducted on the relationship between the Laiziling and Jianfengling plutons. Then, in this paper we report new data of zircon U–Pb dating, bulk-rock

geochemical compositions and zircon Lu–Hf isotopes of Laiziling and Jianfengling granites, aiming to outline the petrogenesis of these two plutons, constrain the source and origin of the granitic magmas, discuss the tectonic setting, and clarify the relationship between these two plutons.

2. Geological Background

The Xianghualing ore field, located in the Chenzhou city, South Hunan province, is one of the biggest Sn–W–Pb–Zn ore fields in China, and consists of Xianghualing Sn deposit (a super-large Sn deposit), Dongshan W deposit (a large W deposit) and many small-medium sized deposits (Figure 2).

The strata, outcropped in the Xianghualing ore field, are composed of Quaternary sediments, Jurassic-Cretaceous sandstone and shale, Carboniferous carbonate and clastic rocks, Mid-Upper Devonian limestone and dolomite, and Permian quartz sandstone and shale, however, the Mid-Upper Devonian rocks are dominant in this area (Figure 2). The faults can be subdivided into five groups, based on theirs trend: NE-, NWW-, NNW-, NW-, NNE-, and EW-trending, however, the NE-trending faults are dominant and acted as the passable and ore-hosting structures in this area (Figure 2, [19]). The intrusive rocks consist of Laiziling, Jianfengling, and some little granitic plutons, and are intruded into the Mid-Upper Devonian limestone and dolomite, and Permian quartz sandstone and shale (Figure 2). Previous studies have revealed that these granitoids are emplaced in Late Jurassic [18], indicating that they were the important part of the Jurassic magmatic activity in South China.
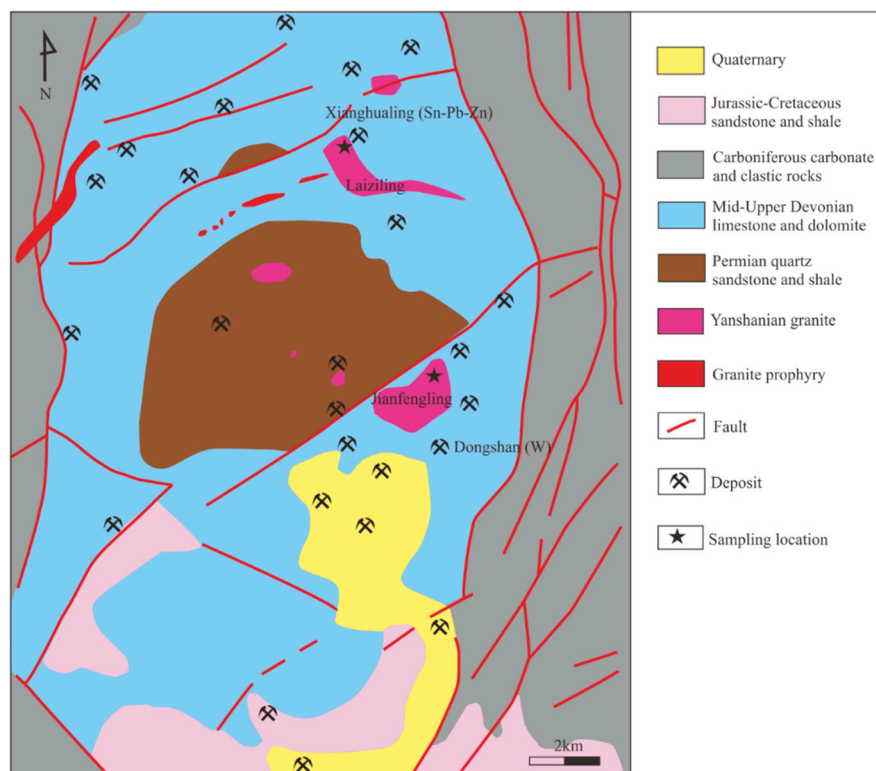
Figure 2. Schematic geological map of the Xianghualing ore field showing the location of samples (modified from [7]).

The Laiziling pluton, occupying an area of 2.2 km^2, is composed of the medium- to coarse-grained two-mica granites. It is characterized by massive-, leucocratic- and porphyroid-texture, and consist of quartz (~40%), K-feldspar (~30%), plagioclase (~20%), biotite (~5%), and muscovite (~5%) (Figure 3a–c). The accessory minerals contain zircon, apatite, sphene, and magnetite. The Jianfengling pluton, occupying an area of 4.4 km^2, is composed of coarse-grained biotite granites. They are also characterized by massive-, leucocratic- and porphyroid-texture, and consists of quartz (~40%),

K-feldspar (~30%), plagioclase (~25%), and biotite (~5%) (Figure 3d–f). The accessory minerals contain zircon, apatite, sphene, and magnetite.
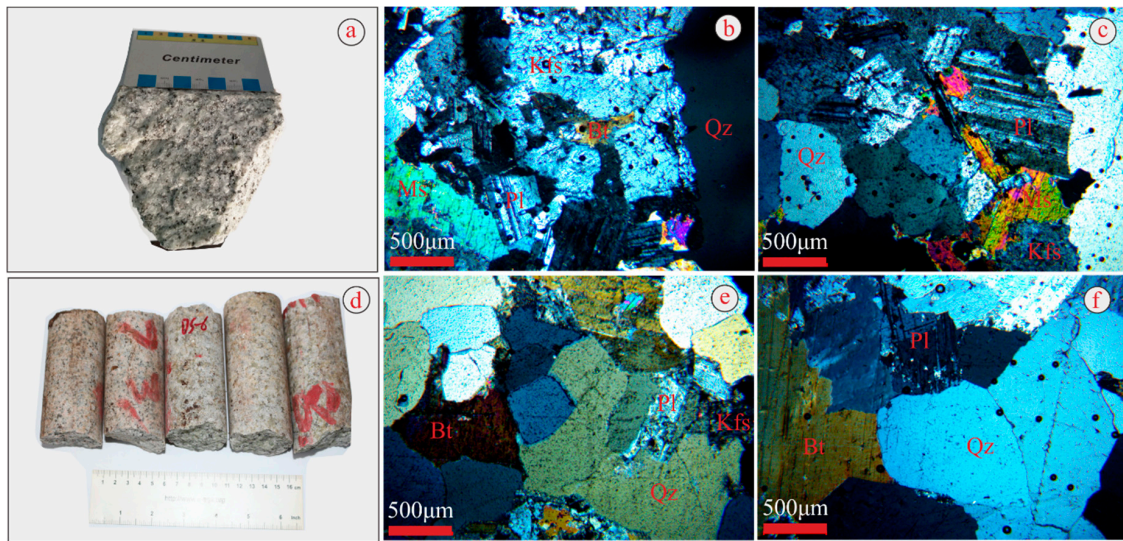
Figure 3. Photos of representative rocks samples (**a**,**d**) and relevant microphotos (**b**,**c**,**e**,**f**). Photos (**a**–**c**) refer to medium-to coarse-grained two-mica granite from Laiziling pluton; Photos (**d**–**f**) refer to coarse-grained biotite granite from Jianfengling pluton. Kfs—K-feldspar; Pl—plagioclase; Qz—quartz; Bt—biotite; Ms—muscovite.

3. Sampling and Analytical Methods

Samples of Laiziling and Jianfengling plutons were collected from drill and underground mine, respectively (Figure 2). Zircon grains used for LA-ICPMS U–Pb dating and Lu–Hf isotopic analyses were separated from a medium- to coarse-grained two-mica granite (sample No. Lzl-1) and a coarse-grained biotite granite (sample No. Ds-6), which were collected from Xianghualing and Dongshan deposits, respectively.

3.1. In Situ LA-ICPMS Zircon U–Pb Dating and Trace Element Compositions

Zircon grains were separated from samples Lzl-1 and Ds-6 using magnetic and heavy liquid separation techniques, and were hand-picked under a binocular microscope before mounted in epoxy resin and polished. Cathodoluminescence (CL) techniques were used to reflect the internal structures of the zircon grains, with a scanning electron microscope (TESCAN MIRA 3 LMH FE-SEM, TESCAN, Brno, Czech Republic) at the Sample Solution Analytical Technology Co., Ltd., Wuhan, China. Zircon grains for U–Pb dating and trace elements analyses were carried out using Laser Ablation Inductively-Coupled Plasma Mass Spectrometry (LA-ICPMS, Agilent, Santa Clara, CA, USA) method at the In situ Mineral Geochemistry Lab, Ore Deposit and Exploration Centre (ODEC), Hefei University of Technology, China. The instrument of an Agilent 7900 Quadrupole ICP-MS coupled to a Photon Machines Analyte HE 193-nm ArF Excimer laser ablation system was used for the analyses. Standard zircon 91500 (1062 ± 4 Ma; [20]) and standard silicate glass (NIST SRM610) was applied to be as external standards for dating and trace element analysis. Quantitative calibration for zircon U–Pb dating and trace elements were performed by ICPMSDataCal 10.7 [21,22], and common Pb was corrected with the model proposed by [23]. Weighted mean age calculation and Concordia diagrams were conducted with the help of an ISOPLOT program from [24].

3.2. Major and Trace Elements Analysis

Bulk-rock major and trace elements analyses were finished at the ALS Geochemistry Laboratory in Guangzhou, China. Before the analyses, samples were crushed in a steel jaw crusher, and then powdered in an agate mill to grain size of 74 μm. The detailed methodology for major element compositions are as follows: Loss of ignition (LOI) was determined after igniting sample powders at 1000 °C for 1 h. A calcined or ignited sample (0.9 g) was added to 9.0 g of Lithium Borate Flux ($Li_2B_4O_7$–$LiBO_2$), mixed well and fused in an auto fluxer between 1050 and 1100 °C. A flat molten glass disk was prepared from the resulting melt. This disk was then analyzed by a Panalytical Axios Max X-ray fluorescence (XRF, Panalytical, Almelo, The Netherlands) instrument, with analytical accuracy of ca. 1–5%.

Trace element compositions were measured using ICP-MS (Perkin Elmer Elan 9000, Perkin, Waltham, MA, USA), after 2-day closed beaker digestion using a mixture of HF and HNO_3 acids in Teflon screw-cap bombs. Detection limits, defined as 3 s of the procedural blank, for some critical elements are as follows (ppm): Th (0.05), Nb (0.2), Hf (0.2), Zr (2), La (0.5) and Ce (0.5). The analytical accuracy is better than 5%.

3.3. Zircon Lu–Hf Isotope Analysis

The zircon Lu–Hf isotopes were conducted on a Neptune Plasma multi-collector inductively coupled plasma mass spectrometer (MC-ICP-MS, NePtune Plus, Thermo Fisher Scientific, Waltham, MA, USA) equipped with New Wave 213 nm FX ArF-excimer laser ablation system, at the laboratory of the Xi'an Institute of Geology and Mineral Resource, Chinese Academy of Geological Sciences, Xi'an, China. Instrumental parameter and data acquisition followed that described by [25,26]. The laser beam diameters were used by 50 μm, 10 Hz repetition rate and 15 J/cm^2 energy density. Helium was used as carrier gas to transport laser eroded matter in Neptune (MC-ICP-MS). Zircon standard GJ-1 was used as external calibration to evaluate the reliability of the analytical data, the recommended $^{176}Hf/^{177}Hf$ ratio of 0.282006 ± 24 (2σ, [26]). Isobaric interference of ^{176}Lu on ^{176}Hf was corrected measuring the intensity of the interference-free ^{175}Lu isotope and using a recommended $^{176}Lu/^{175}Lu$ ratio of 0.02655 (2σ, [27]). Similarly, the isobaric interference of ^{176}Yb on ^{177}Hf was corrected against the $^{176}Yb/^{172}Yb$ ratio of 0.5886 (2σ, [28]) to calculate $^{176}Hf/^{177}Hf$ ratios. In doing so, a normalizing $^{173}Yb/^{171}Yb$ ratio of 1.12346 for the analyzed spot itself was automatically used in the same run to calculate a mean $β_{Yb}$ value, and then the ^{176}Yb signal intensity was calculated from the ^{173}Yb signal intensity and the mean $β_{Yb}$ value [29,30]. In this work, we adopted the decay constant for ^{176}Lu of $1.865 × 10^{-11}$ a^{-1} [31], the present-day chondritic ratios of $^{176}Hf/^{177}Hf$ = 0.282772 and $^{176}Lu/^{177}Hf$ = 0.0332 [32], the present-day depleted mantle value of $^{176}Hf/^{177}Hf$ = 0.28325 [33] and $^{176}Lu/^{177}Hf$ = 0.0384 [34]. All the Lu–Hf isotope results are reported in 2σ error. The data processing and related parameters calculation was finished with the help of an Excel program "Hflow".

4. Results

4.1. Zircon U–Pb Dating

Most of the zircons from medium- to coarse-grained two-mica granite (sample No. Lzl-1) of Laiziling pluton are euhedral, with obvious internal oscillatory zoning in CL images (Figure 4a), indicating a magmatic origin of these zircons [35]. The length of these zircons are from 60 to 150 μm with length-to-width ratios of 1:1 to 3:1. The contents of U and Th are 402–4683 ppm (mean = 1209 ppm) and 232–2132 ppm (mean = 615 ppm), with Th/U ratios of 0.44–0.73 (mean = 0.55), which also indicate that they were typical magmatic zircons [35]. The $^{206}Pb/^{238}U$ ages of fourteen zircons vary from 152.5 Ma to 166.4 Ma which plot on or near the concordant curve (Supplementary Materials Table S1), and a weighted mean $^{206}Pb/^{238}U$ age of 156.4 ± 1.4 Ma (MSWD = 1.6) was yielded (Figure 4b).

Most of the zircons from coarse-grained biotite granite (sample No. Ds-6) of Jianfengling pluton are also featured by euhedral and obvious internal oscillatory zoning in CL images (Figure 4c),

indicating a magmatic origin of these zircons [35]. The length of these zircons are from 50 to 200 µm with length-to-width ratios of 1:1 to 3:1. The contents of U and Th are 177–2779 ppm (mean = 954 ppm) and 94–1732 ppm (mean = 498 ppm), with Th/U ratios of 0.38–0.76 (mean = 0.55), which also indicate that they were typical magmatic zircons [35]. The ^{206}Pb/^{238}U ages of twenty-two zircons vary from 160.1 Ma to 170.7 Ma which plot on or near the concordant curve (Supplementary Materials Table S1), and a weighted mean ^{206}Pb/^{238}U age of 165.2 ± 1.4 Ma (MSWD = 0.47) was obtained (Figure 4d).
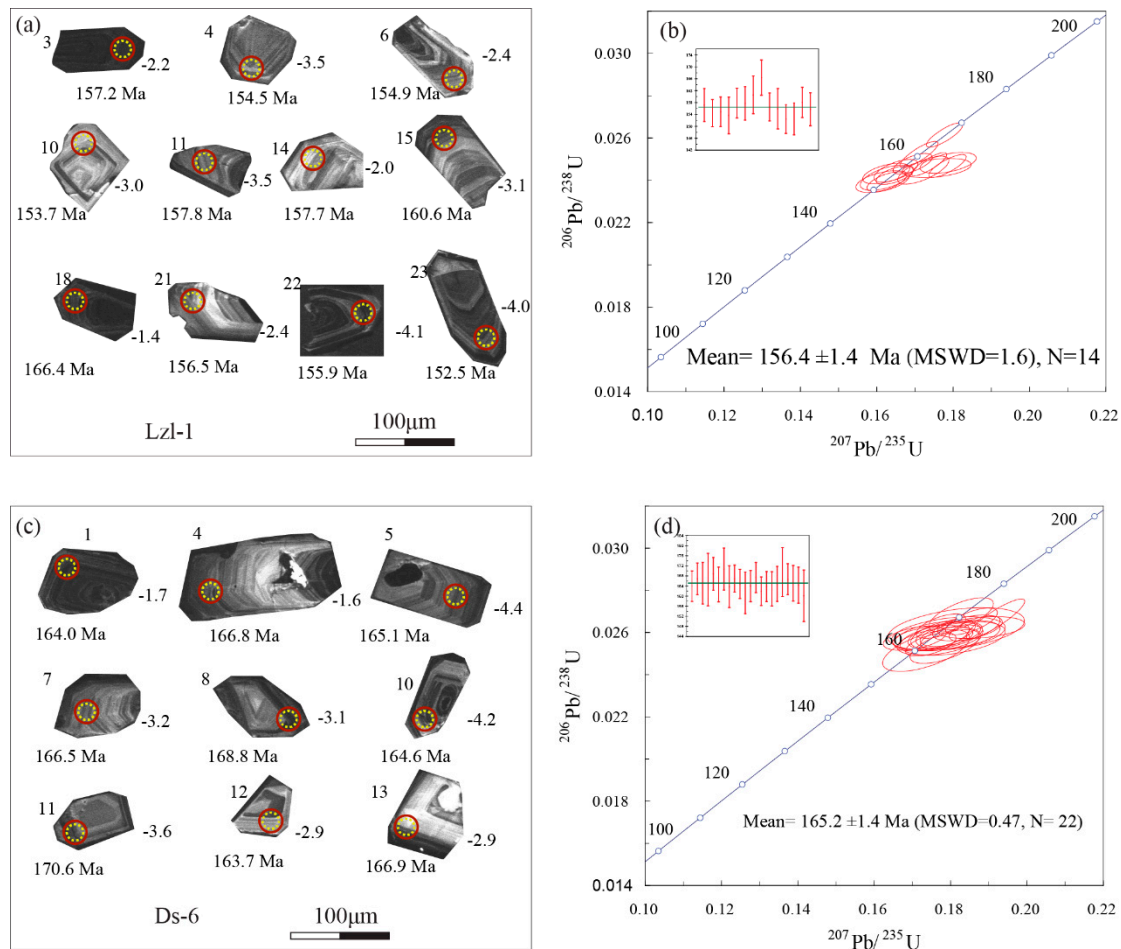

Figure 4. Cathodoluminescence (CL) images of zircon grains (**a**,**c**) and concordant diagrams of zircon U–Pb ages (**b**,**d**) from the Laiziling and Jianfengling granites, respectively. Red and yellow circles are spots for the zircon U–Pb dating and Lu–Hf isotopes analyses, respectively in (**b**,**d**).

4.2. Trace Element Compositions of Zircons

The trace element compositions of zircon grains are listed in Supplementary Materials Table S2. Zircon grains of sample Lzl-1 have relatively high contents of Ti and REEs (rare earth elements), and are from 4.09 to 11.99 ppm (mean = 8.41 ppm) and from 593 to 1440 ppm (mean = 1026 ppm), respectively. They are enriched in HREEs (heavy rare earth elements) and depleted in LREEs (light rare earth elements), with LREE/HREE ratios of 0.02–0.04 (mean = 0.03). The chondrite normalized REE patterns are featured by left-leaning steep slopes, and obvious positive Ce anomalies (Ce/Ce* = 7.03–30.52, mean = 15.57), and negative Eu anomalies (Eu/Eu* = 0.01–0.06, mean = 0.03, Figure 5a).

Zircon grains from sample Ds-6 have a little higher Ti and REE contents than those of sample Lzl-1, with Ti content of 3.71–18.31 (mean = 10.27) and REE content of 479–1691 (mean = 956). They also are enriched in HREEs and depleted in LREEs, with LREE/HREE ratios of 0.02–0.04 (mean = 0.03). The chondrite normalized REE patterns are featured by left-leaning steep slopes, and obvious positive

Ce anomalies (Ce/Ce* = 5.35–34.21, mean = 18.41), and negative Eu anomalies (Eu/Eu* = 0.01–0.11, mean = 0.04, Figure 5b).
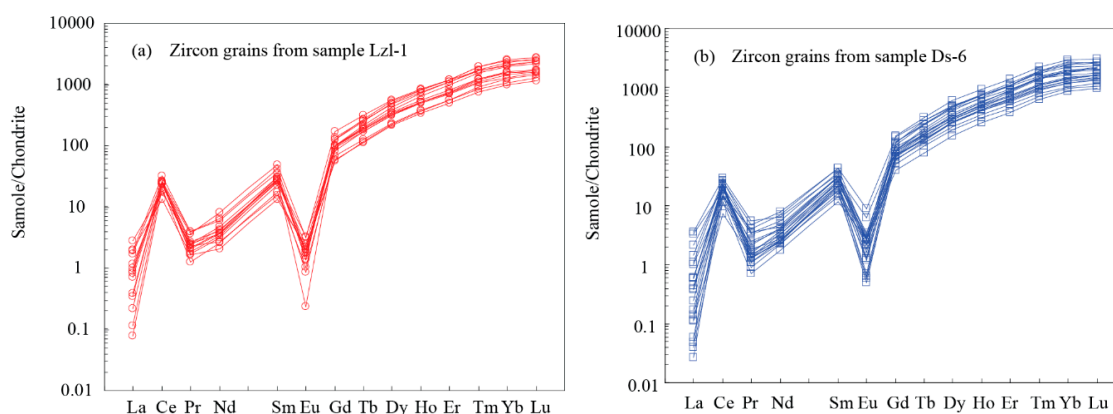

Figure 5. Chondrite-normalized REE (rare earth element) chemistry of zircon grains for the samples taken from the Laiziling (**a**) and Jianfengling (**b**) plutons, with normalizing factors from [36].

4.3. Major and Trace Element Compositions

Major and trace element compositions of the granites from Laiziling and Jianfengling plutons are presented in Supplementary Materials Table S3. The Laiziling granites are characterized by high contents of SiO_2 (73.92–74.61%, mean = 74.36%), Al_2O_3 (13.62–14.26%, mean = 13.90%), Na_2O (3.66–3.95%, mean = 3.81%), and K_2O (3.61–4.20%, mean = 3.89%) and low contents of TiO_2 (0.02–0.03%, mean = 0.03%), MgO (0.06–0.09%, mean = 0.08%), and P_2O_5 (0.01%). The Jianfengling granites have the similar major element composition to that of the Laiziling granites, characterized by high contents of SiO_2 (74.07–75.38%, mean = 74.79%), Al_2O_3 (13.19–13.86%, mean = 13.46%), Na_2O (2.05–5.08%, mean = 3.16%) and K_2O (2.38–4.21%, mean = 3.08%), and low contents of TiO_2 (0.01–0.04%, mean = 0.03%), MgO (0.01–0.07%, mean = 0.05%) and P_2O_5 (0.01%). In addition, all the samples are plotted in the field of granite in the SiO_2 vs. $Na_2O + K_2O$ diagram, indicating that these two-rock types are both typical granites (Figure 6). All the samples from Laiziling pluton are plotted in the field of high-K calc-alkaline, however, the samples from Jianfengling pluton are plotted in the field of high-K calc-alkaline and calc-alkaline (Figure 7a). Both of the granites have high A/CNK (molar $Al_2O_3/(CaO + Na_2O + K_2O)$) values, with Laiziling granites of 1.17–1.23 (mean = 1.19) and Jianfengling granites of 1.06–1.64 (mean = 1.36), respectively, indicating that they belong to peraluminous series (Figure 7b). They also have high differentiation index values (DI), ranging from 91 to 93 (mean = 92) and from 84 to 94 (mean = 89) for the Laiziling and Jianfenging granites, respectively.

Both of the granites from Lalziling pluton and Jianfengling pluton have similar trace element contents and primitive-mantle normalized patterns, which are enriched in Rb, U, Nb, and Sm, and depleted in Ba, Sr, P, and Ti (Figure 8a). They also have the similar REE contents and chondrite normalized patterns, with ΣREEs of 341–370 ppm (mean = 358 ppm) and of 297–425 ppm (mean = 329 ppm) for the Laiziling and Jianfengling granites, respectively (Figure 8b). They also have obvious negative Eu anomalies, with Eu/Eu* values of 0.01 for granites from both of the plutons.
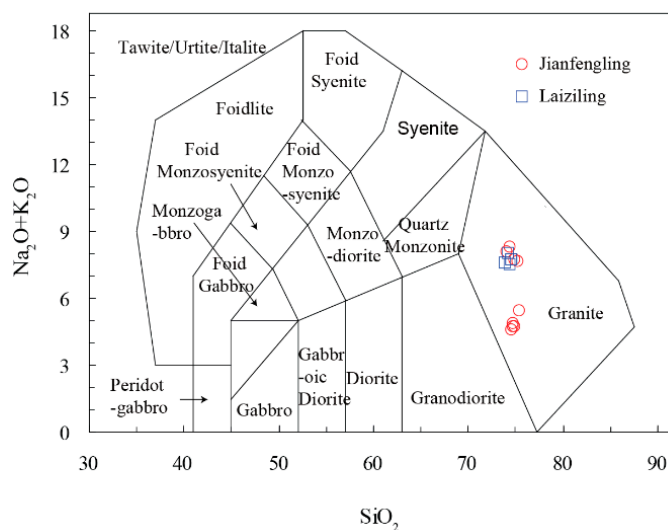
Figure 6. Classification diagram of igneous rocks for the samples from the Laiziling and Jianfengling plutons (modified from [37]).
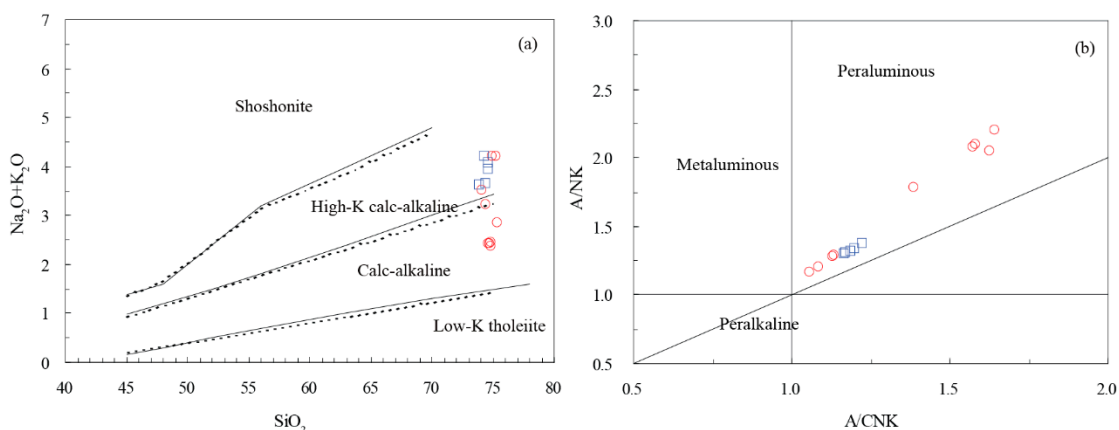

Figure 7. SiO_2 versus $Na_2O + K_2O$ (**a**) and A/CNK versus A/NK (**b**) diagrams for the samples from the Laiziling and Jianfengling plutons (**a** and **b** are modified from [38,39], respectively). Symbols are as in Figure 6. A/CNK = molar $Al_2O_3/(CaO + Na_2O + K_2O)$; A/NK = molar $Al_2O_3/(Na_2O + K_2O)$.
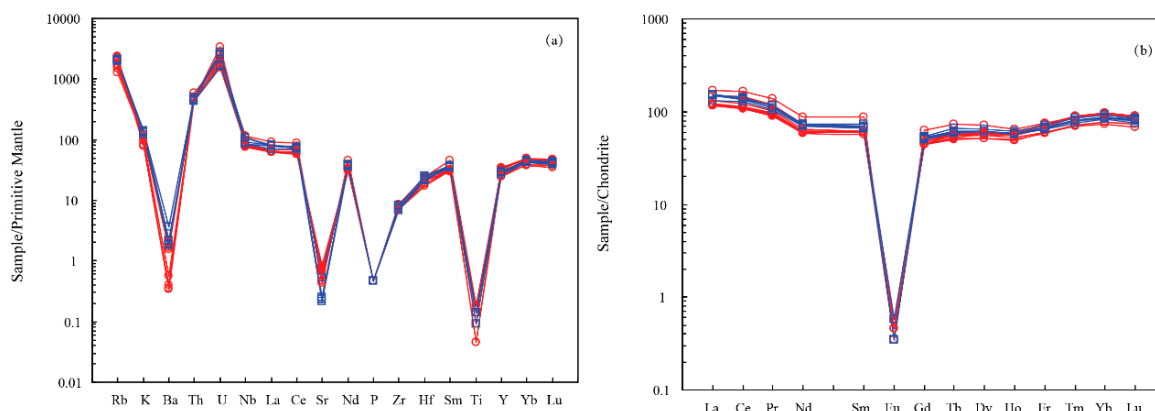
Figure 8. Primitive-mantle-normalized trace element (**a**) and chondrite-normalized REE (**b**) variation diagrams for samples from the Laiziling and Jianfengling plutons. Normalizing factors are from [36,40], respectively. Symbols are as in Figure 6.

4.4. Zircon Lu–Hf Isotopic Compositions

The zircon Lu–Hf isotopic compositions and related parameters for the granites from Laiziling pluton (sample No. Lzl-1) and Jianfengling pluton (sample No. Ds-6) are listed in Supplementary Materials Table S4. Result for the sample Lzl-1 have variable $^{176}Lu/^{177}Hf$ ratios of 0.000572–0.007548, and similar present-day $^{176}Hf/^{177}Hf$ ratios of 0.282562–0.282658. The calculated initial $^{176}Hf/^{177}Hf$ (Hf$_i$) ratios vary from 0.282559 to 0.282636, with $\varepsilon_{Hf}(t)$ values of −3.86 to −1.38 (mean = −2.91) and T$_{DMC}$ages of 1.30 to 1.47 Ga (mean = 1.39 Ga), which were calculated by the zircon U–Pb age of 156.4 Ma (Figure 9a,b).
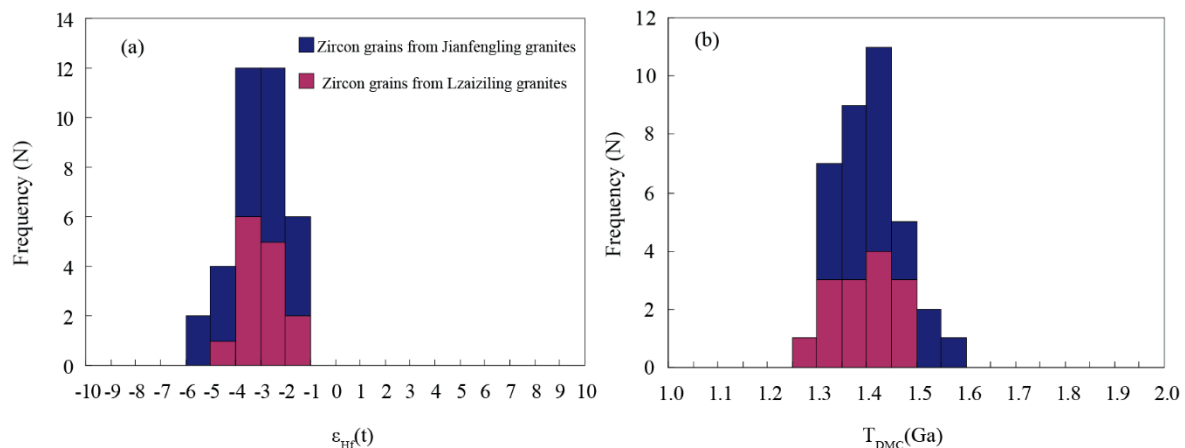
Figure 9. Statistical histograms for $\varepsilon_{Hf}(t)$ (**a**) and T$_{DMC}$ (**b**)values for the zircon grains from the Laiziling and Jianfengling plutons.

Zircon spots from sample Ds-6 also show variable $^{176}Lu/^{177}Hf$ ratios of 0.000429–0.003164 and similar present-day $^{176}Hf/^{177}Hf$ ratios of 0.282520–0.282630. The calculated initial $^{176}Hf/^{177}Hf$ (Hf$_i$) ratios vary from 0.282516 to 0.282625, with $\varepsilon_{Hf}(t)$ values of −5.44 to −3.71 (mean = −3.17) and T$_{DMC}$ ages of 1.32 to 1.56 Ga (mean = 1.42 Ga), which were calculated by the zircon U–Pb age of 165.2 Ma (Figure 9a,b).

5. Discussion

### 5.1. Genetic Type of the Granitic Rocks: An A-Type Affinity

The issue on the classification of the granitic rocks has been a hot topic for decades, and many types of granitic rocks are proposed based on the different standards, among which the classification of I-, S-, M-, and A-type granite are well accepted all over the world [41–51]. The term of A-type granite was first proposed by [45] and defined by their alkaline, anhydrous and anorogenic nature. Then, many geologists enriched and improved the concept of A-type granite, making it a significant component of the granite series [44,52–55]. Generally, in terms of the elemental compositions, the A-type granites have high contents of SiO$_2$, K$_2$O, Na$_2$O, Zr, Nb, REE, Y, and Ga, and low contents of CaO, Sr, Ba, and so forth, and characterized by high ratios of Ga/Al and (K$_2$O + Na$_2$O)/CaO [43]. The Laiziling and Jianfengling granites are characterized by high contents of SiO$_2$ (average ca. 74%), total alkalis (K$_2$O + Na$_2$O, average ca. 6.9%), total REE, and Ga, with depletion in Sr and Ba, which are similar to the major- and trace-element compositions of A-type granites [43]. Both of the Laiziling and Jianfengling granites have high 10,000 Ga/Al ratios, most of which are higher than 4, and are plotted in the field of A-type granite in the related discrimination diagrams (Figure 10). In addition, the extremely low content of P$_2$O$_5$ (0.01%) for the Laiziling and Jianfengling granites which differs from the typical S-type granites indicates that they might not belong to S-type granite [46]. The peraluminous nature, which most of A/CNK ratios are higher than 1.1, indicates that these granites are unlikely I-type

granite [47]. Furthermore, the high content of FeO^t, K$_2$O, and Na$_2$O and low content of MgO also reveal that they might be likely A-type granites, since most of the samples are plotted in the field of A-type granites (Figure 11) [56,57].

Recent studies have revealed that most of the late Mesozoic granitic plutons in Nanling were mainly composed of the A-type granites, forming a NE-trending granite belt [58,59]. Generally, granites of this belt in Nanling were exposed at the central of the Shi-Hang zone proposed by [58] (Figure 1a). In addition, numerous A-type granitic plutons have been identified in the past few decades along the Shi-Hang zone, including Guposhan [60], Xitian [61], Qitianling [62], Laiziling [63], and so on. Consequently, geochemical characters of Laiziling and Jianfengling granites, together with the regional geology of the Jurassic granites along the Shi-Hang zone, reveal that they have an affinity of A-type rather than S- and I-type granite.
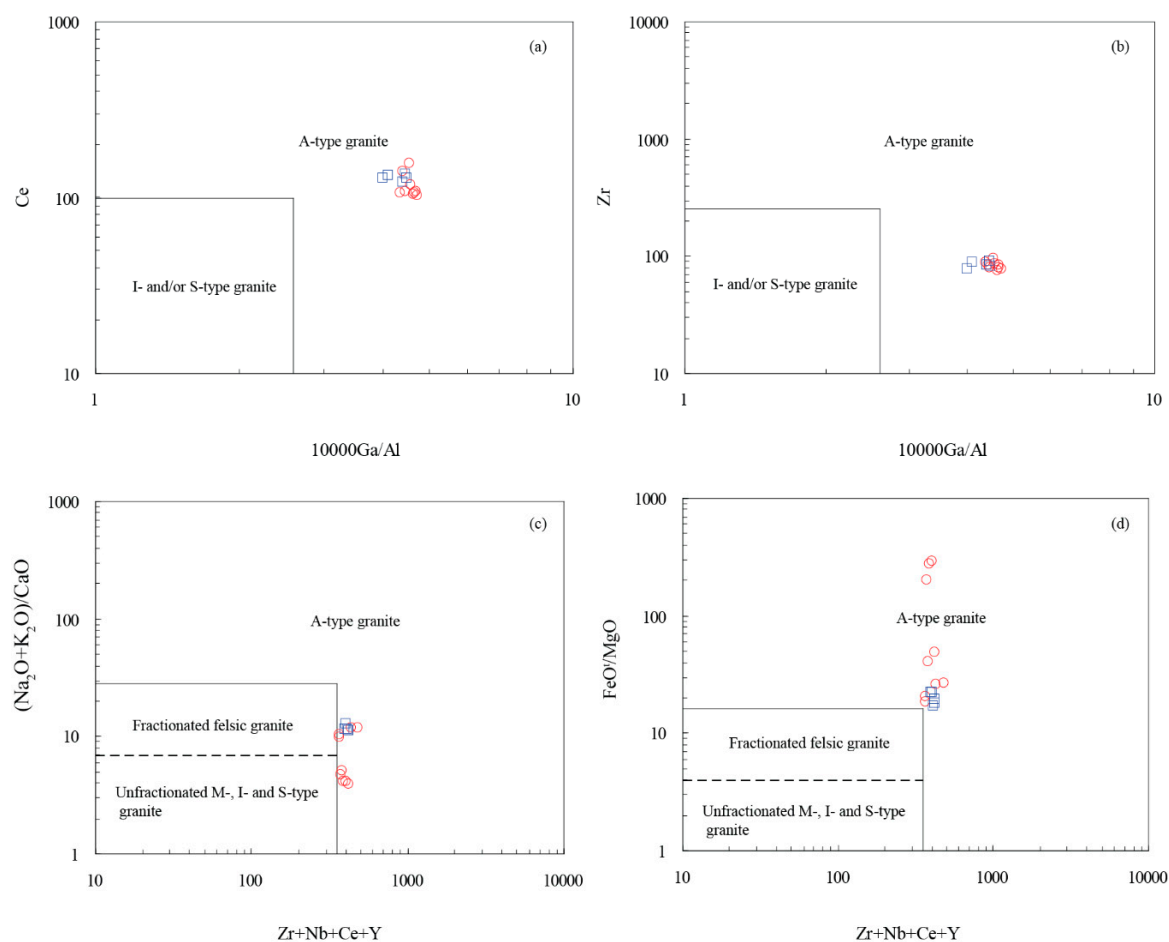
Figure 10. Discrimination diagrams on the types of granites from the Laiziling and Jianfengling plutons (modified from [43]). (**a**) 10000 Ga/Al versus Ce; (**b**) 10000 Ga/Al versus Zr; (**c**) Zr + Nb + Ce + Y versus (Na$_2$O + K$_2$O)/CaO; (**d**) Zr + Nb + Ce + Y versus FeO^t/MgO. Symbols are as in Figure 6.
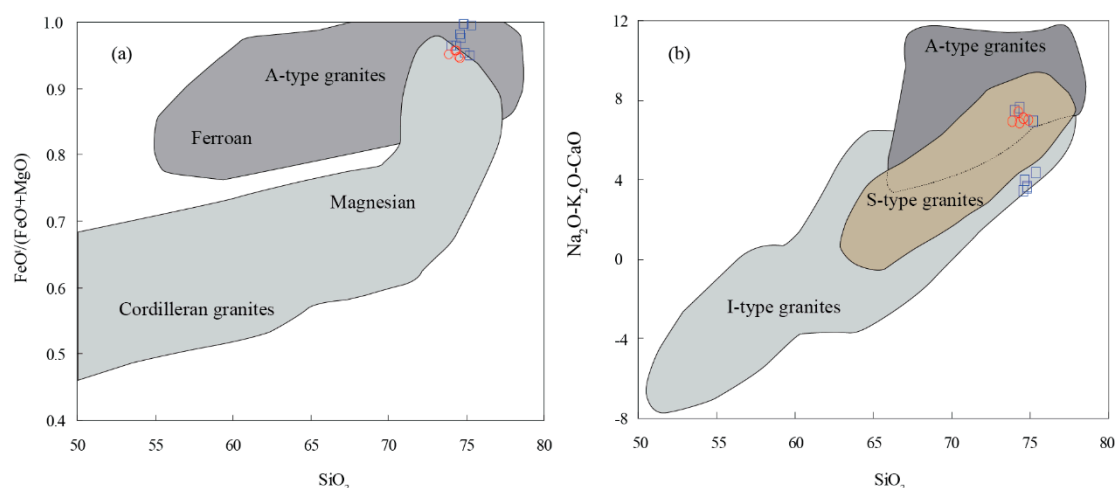
Figure 11. Discrimination diagrams on the types of granites from the Laiziling and Jianfengling plutons (modified from [56]). (**a**) SiO_2 versus $FeO^t/(FeO^t + MgO)$; (**b**) SiO_2 versus $Na_2O + K_2O - CaO$. Symbols are as in Figure 6.

5.2. Genesis of Laiziling and Jianfengling Granites
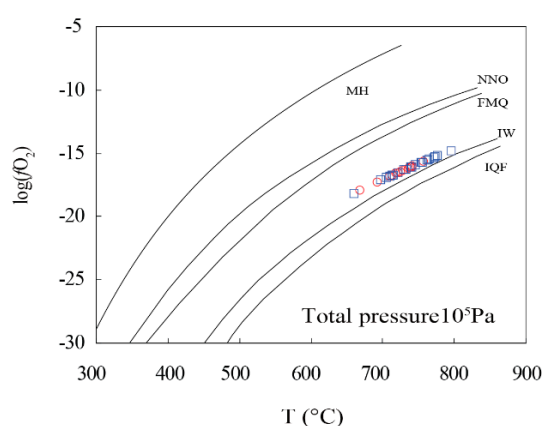
5.2.1. Temperatures

Temperature is a significant index to reflect the magma process and the genesis of granites [42,64–68]. As one of the most stable minerals in igneous rocks, zircons can be resistant to a certain degree of weathering and alteration in many kinds of geological events. In addition, the Zr partition coefficient and Ti content in zircon is sensitive to the temperature [65,67–69]. Then, based on those theories, [68] conducted an experiment on the solubility of Zr in melt at 860, 930 and 1020 °C and a model of zircon saturation thermometer was proposed to estimate the temperature of magmatic melt. Based on the crystal growth experiments of zircon in siliceous melt at different levels of temperature, the zircon Ti thermometer was first proposed by [69]. Furthermore, Ferry et al. [65] revised and replenished the model, making it an important and useful tool to reflect the temperatures of magmatic melt.

Then, in order to probe into the temperatures of Laiziling and Jianfengling granites, we used these two calculation models to estimate the temperatures of these granites. The results show that the calculated temperatures range from 738 to 751 °C (mean = 743 °C) and from 708 to 749 °C (mean = 725 °C) for the Laiziling and Jianfengling granites, respectively, with the help of zircon saturation thermometer (Supplementary Materials Table S3). The results calculated by zircon Ti thermometer show the similar temperatures for the Laiziling and Jianfengling granites, ranging from 668 to 757 °C (mean = 724 °C) and from 661 to 797 °C (mean = 739 °C), respectively (Supplementary Materials Table S2). The consistent temperatures, based on both of the calculated models, indicate that the both of Laiziling and Jianfengling granites crystalized from magmas with relatively high temperature (ca. 730 °C). Furthermore, the evidence that the zircons from both the Laiziling and Jianfengling granites lack of inherited core reveals that these temperatures can be as the minimum estimation for the magmatic melts.

5.2.2. Oxygen Fugacities and Fractional Crystallization

Similar to the temperature, oxygen fugacity is also a significant index to reflect the redox condition of magma melt, not only for the genesis of granites but also for their close relationship with the mineralization of different metals [60,70–81]. For example, high oxygen fugacity plays an important role in controlling the formation of porphyry Cu–Au and epithermal Au–Cu deposits, whereas, low oxygen fugacity is in favor of the W–Sn–Mo mineralization [75,76,79,82]. Recent studies revealed

that some elements (Eu, Ce, and so on) in zircon can be an efficient tracers to reflect the oxidation status of magma [70,80,83]. Since the Eu and Ce are multivalent elements, with Eu^{2+} and Eu^{3+} for Eu, and Ce^{4+} and Ce^{3+} for Ce, respectively. Since valence of Ce and Eu is sensitive to the redox conditions of the melt, then the Ce^{4+}/Ce^{3+} and Eu^{3+}/Eu^{2+} ratios can be a useful parameters to reflect the redox conditions of the melt [84]. Based on the results from an experiment at different levels of temperature and oxygen fugacity, [80] proposed a model to calculate the oxygen fugacity of magma during zircon crystallization. The calculation results show that both of the Laiziling and Jianfengling granites have similar oxygen fugacities, with $\log(fO_2)$ values of -18 to -15.7 (mean $= -16.5$) and -18.2 to -14.8 (mean $= -16.2$), respectively. In addition, almost all the samples from both of these two plutons are plotted in the field between the IW (iron-wustite)- and FMQ (fayalite-magnetite-quartz)- buffer, and were close to the IW-buffer in the T versus $\log(fO_2)$, indicating that they have relatively low oxygen fugacities (Figure 12). Then, based on the evidences above, we can conclude that the Laiziling and Jianfengling granites were crystalized from a reducing magma.

Figure 12. Temperature (°C) versus $\log(fO_2)$ diagram for the zircon grains from the Laiziling and Jianfengling granites (modified from [85]). Symbols are as in Figure 6. MH (magnetite-hematite); NNO (Ni-NiO); FMQ (fayalite-magnetite-quartz); IW (iron-wustite); IQF (iron-quartz-fayalite).

The fractional crystallization process has been proved by the depletion of P, Ta, Sr, Ti, Ba, and Eu of these granites, which represents the fractional crystallization of plagioclase, apatite, ilmenite, K-feldspar, and other minerals (Figure 8a,b). In addition, the positive correlation between the Rb and Ba and negative correlation between Rb and Sr suggest that the fractional crystallization of plagioclase and biotite is significant during the evolution of magma process (Figure 13a,b).
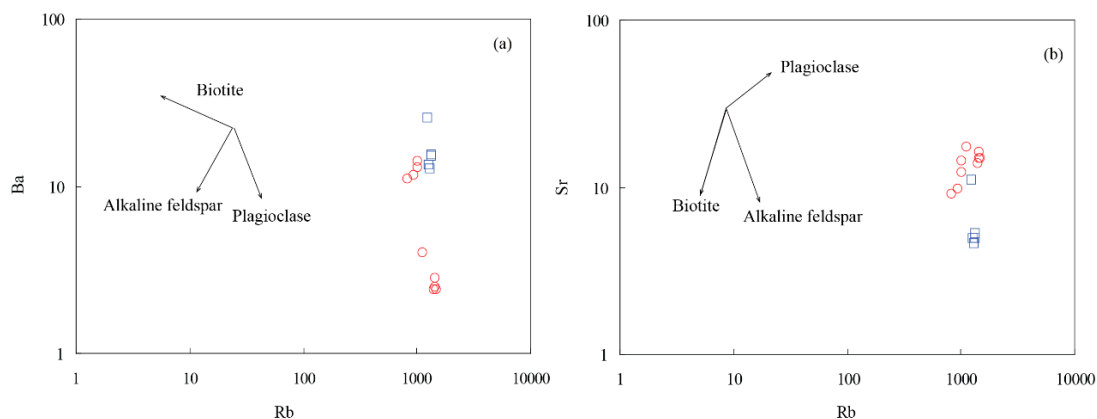

Figure 13. Rb versus Ba (**a**) and Rb versus Sr (**b**) diagrams for the Laiziling and Jianfengling granites. Symbols are as in Figure 6.

5.2.3. Magma Source

The source and genesis of A-type granite have long been a debatable topic for decades, and many models have been proposed to explain that, for example, fractional crystallization of mantle-derived magma [41], partial and/or complete melting of granulite [41], partial and/or complete melting of calc-alkali metasomatized mantle [54], partial melting of old granodiorite [86], partial melting of crust [43,52,87], and magma mixing [88,89].

The elemental compositions of the Laiziling and Jianfengling granites reveal that they were unlikely originated from the fractional crystallization of mafic rocks, and the model of fractional crystallization of mafic magma can rule out. The A-type granite nature of these granites can rule out the model of partial melting of old granodiorite which is mainly I-type granites. In addition, these granites are aluminous A-type granites with high A/CNK ratios, and the aluminous A-type granites could be generated from the partial melting of a felsic infracrustal source [42]. The Lu–Hf compositions of these granites from Laiziling and Jianfengling plutons are characterized by negative $\varepsilon_{Hf}(t)$ values (mean = −2.91 and −3.17, respectively) and old T_{DMC} ages (mean = −1.39 Ga and 1.42 Ga, respectively), indicating that they were likely mainly originated from a crustal source. However, the Lu–Hf isotopic features of Laiziling and Jianfengling granites differ from these coeval granites which were originated from the partial melting of the Proterozoic basement with no and/or few mantle materials involved in the Nanling range, such as Taoxikeng [90], Dengfuxian [91], and Xihuashan plutons [92] (Figure 14a,b). In addition, the Lu–Hf isotopic features of Laiziling and Jianfengling granites are similar to these coeval granites which were originated from the mixing of mantle and crustal materials, such as Jiuyishan [93], Guposhan [94] and Qitianling plutons [62] (Figure 14a,b). Thus, we can conclude that the Laiziling and Jianfengling plutons might likely be originated from the partial melting of Proterozoic basement of South China with a certain amount of mantle-derived magma involved.
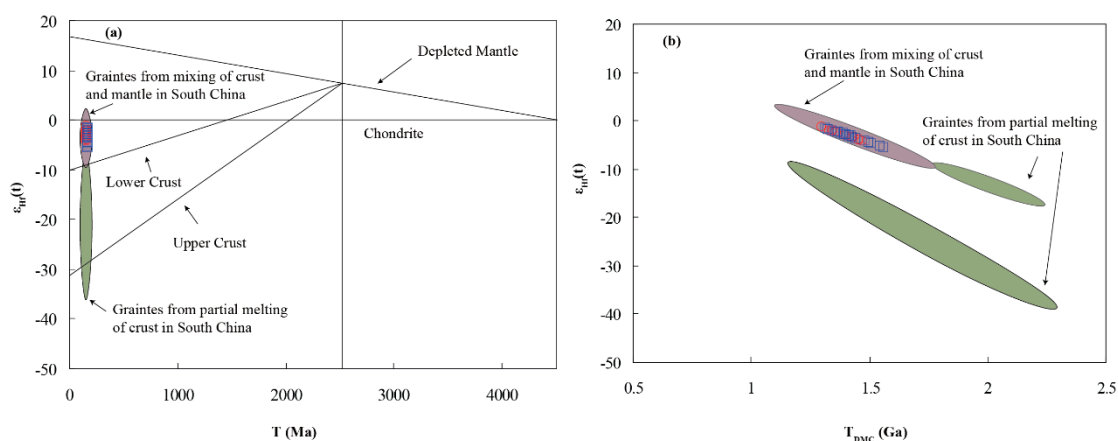
Figure 14. (**a**) Age versus $\varepsilon_{Hf}(t)$ and (**b**) T_{DMC} versus $\varepsilon_{Hf}(t)$ plots for the samples from the Laiziling and Jianfengling plutons. Data of granites from mixing of crust and mantle are from [62,93,94]; Data of granites from partial melting of crust in South China are from [90–92]. Symbols are as in Figure 6.

5.2.4. Relationship between the Two Granitic Plutons and Genesis of Laiziling and Jianfengling Granites

As stated above, we obtain two zircon ages for the Laiziling and Jianfengling granites, which are 156.4 ± 1.4 Ma and 165.2 ± 1.4 Ma, respectively, and these ages are consistent with the former studies within the uncertainty [17,63]. However, the relationship between the two granitic rocks were poorly understood, since they have an age interval of ca. 10 Ma during the emplacement of magma. Then, in order to probe into the relation between the two granitic plutons, some evidence we should ignore includes: (1) the similar major element compositions with high contents of SiO_2,

Al$_2$O$_3$, Na$_2$O, and K$_2$O, low contents of TiO$_2$, MgO, and P$_2$O$_5$; (2) terrifically similar trace element primitive-mantle normalized patterns and REE chondrite normalized patterns; and (3) nearly parallel zircon Lu–Hf isotopic compositions. These proofs indicate that both of the Laiziling and Jianfengling plutons might be originated from the same magma chamber, although, their emplaced age of Laiziling pluton is ca. 10 Ma after that of Jianfengling pluton. The new evidence was also provided by the mineral compositions with the occurrence of muscovite in Laiziling granites rather than in Jianfengling granites, since the residual magma will be enriched in Al, Si, K, Na, and so on, during the process of fractional crystallization.

Then, together with the evidences above, the genesis of the Laiziling and Jianfengling plutons might be concluded as following: (1) primary magma chamber was formed from mixing of partial melting of Proterozoic basement and a certain amount of mantle-derived magma; (2) the magma uplifted and intruded into the Paleozoic strata in ca. 165 Ma and Jianfengling pluton formed; and (3) during the process of fractional crystallization, the residual magma which was enriched in Al, uplifted and emplaced in ca. 156 Ma leading to the formation of Laiziling pluton.

5.3. Tectonic Settings

The tectonic settings of A-type granite have been a hot spot for decades, however, an overwhelming number of studies have revealed that A-type granites were formed in extensional settings, such as intraplate rift, mantle plume, back-arc extension, post-collisional extension and so on [43,45,54]. In addition, the A-type granite can be subdivided into two types of granites: A1-type granite associated with the intraplate rift and/or mantle plume and A2-type granite associated with back-arc extension, intraplate extension, and/or post-collisional extension [95]. Based on the discrimination diagrams from [95], the Laiziling and Jianfengling granites are all plotted in the field of A2-type granite, indicating that these granites belong to A2-type granite which are likely associated with the back-arc extension, intraplate extension, and/or post-collisional extension (Figure 15a,b). Furthermore, these granites are plotted in the field of within plate granite (WPG) in the diagrams proposed by [96], indicating an intraplate setting for these granites (Figure 15c,d). The results demonstrate that the Laiziling and Jianfengling granites might likely be emplaced in an intraplate extensional setting. As a part of Jurassic tectonic-magmatic activity in South China, the Laiziling and Jianfengling plutons might be formed in the same tectonic setting with other coeval granitic plutons, such as Qitianling, Guposhan, and Jiuyishan plutons [62,93,94]. However, the geodynamic mechanism triggering the extensional setting and magma activity in South China has long been in debate for decades [59,97–107]. Several models have been proposed to illustrate the geodynamic mechanism, for example, westward subduction of the paleo-pacific plate, mantle plume, post-collision, and so on [97–101,104,105,107]. However, these models concede that the tectonic setting of South China in Jurassic is an extensional setting, and the process of lithospheric extension and thinning occurred in that period [108,109]. Furthermore, these two plutons are located near the Shi-hang zone, which was recognized as the collision belt between the Yangtze and Cathaysia Blocks, and some unsubstantial spots can be the tunnel for the upwelling and emplacement of the mantle magma to mix with the crustal melt.
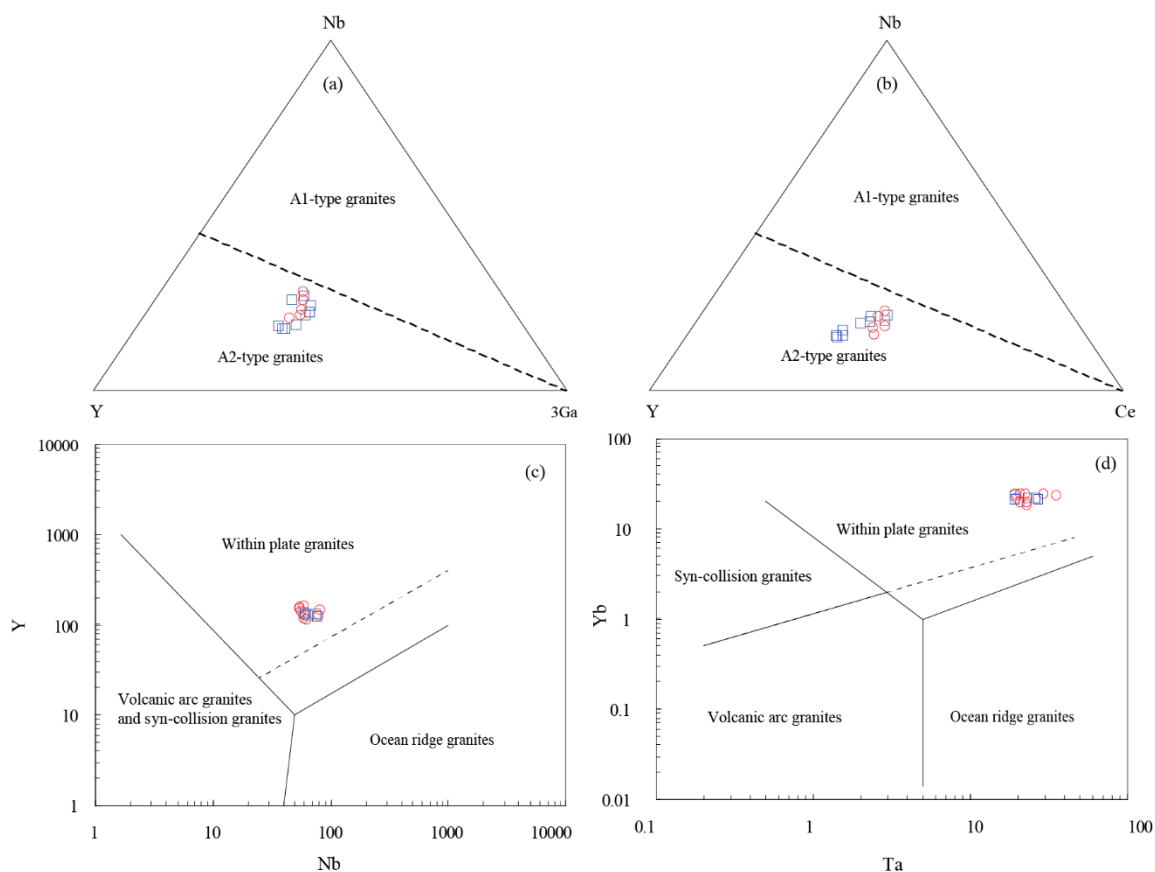
Figure 15. (**a**) Nb–Y–3Ga and (**b**) Nb–Y–Ce triangular diagrams; (**c**) Nb versus Y and (**d**) Ta versus Yb diagrams for the granites from the Laiziling and Jianfengling plutons. (**a**,**b**) are modified from [43]; (**c**,**d**) are modified from [96]. Symbols are as in Figure 6.

6. Conclusions

1. Zircon U–Pb dating yielded precise crystallization ages of 156.4 ± 1.4 Ma and 165.2 ± 1.4 Ma for the Laiziling and Jianfengling plutons in South Hunan, respectively.
2. Both of the Laiziling and Jianfengling granites are high-K, strongly peraluminous, and highly fractionated A-type granites with high temperatures and low oxygen fugacity. They were mainly originated from the Proterozoic basement of South China with a certain amount of mantle-derived magma involved.
3. The Laiziling and Jianfengling plutons were derived from the same magma chamber, and were the products of magma emplacement successively.
4. The granitic magma was emplaced in an extensional setting.

Author Contributions: X.W. and J.C. conceived and designed the experiments; B.H. and X.Z. took part in the discussion; Y.G. and W.S. took part in the field campaigns; L.Y., X.W. and J.C. wrote the paper.

Conflicts of Interest: The authors declare no conflict of interest.

References

1. Zhao, J.; Zhou, M.; Yan, D.; Zheng, J.; Li, J. Reappraisal of the ages of Neoproterozoic strata in South China: No connection with the Grenvillian orogeny. *Geology* **2011**, *39*, 299–302. [CrossRef]

2. Cao, J.Y.; Yang, X.Y.; Du, J.G.; Wu, Q.H.; Kong, H.; Li, H.; Wan, Q.; Xi, X.S.; Gong, Y.S.; Zhao, H.R. Formation and geodynamic implication of the Early Yanshanian granites associated with W–Sn mineralization in the Nanling range, South China: An overview. *Int. Geol. Rev.* **2018**. [CrossRef]

3. Yang, M.G.; Mei, Y.W. Characteristics of geology and metallization in the Qinzhou-Hangzhou paleoplate juncture. *Geol. Miner. Resour. South China* **1997**, *3*, 52–59. (In Chinese)

4. Li, H.Y.; Mao, J.W.; Sun, Y.L.; Zou, X.H.; He, H.L.; Du, A.D. Re–Os isotopic chronology of molybdenites in the Shizhuyuan polymetallic tungsten deposit, Southern Hunan. *Geol. Rev.* **1996**, *42*, 261–267.

5. Li, H.; Yonezu, K.; Watanabe, K.; Tindell, T. Fluid origin and migration of the Huangshaping W–Mo polymetallic deposit, South China: Geochemistry and Ar-40/Ar-39 geochronology of hydrothermal K-feldspars. *Ore Geol. Rev.* **2017**, *86*, 117–129. [CrossRef]

6. Lu, Y.; Ma, L.; Qu, W.; Mei, Y.; Chen, X. U–Pb and Re–Os isotope geochronology of Baoshan Cu–Mo polymetallic ore deposit in Hunan province. *Acta Petrol. Sin.* **2006**, *22*, 2483–2492. (In Chinese)

7. Yuan, S.; Peng, J.; Hu, R.; Li, H.; Shen, N.; Zhang, D. A precise U–Pb age on cassiterite from the Xianghualing tin-polymetallic deposit (Hunan, South China). *Miner. Depos.* **2008**, *43*, 375–382. [CrossRef]

8. Peng, J.; Zhou, M.; Hu, R.; Shen, N.; Yuan, S.; Bi, X.; Du, A.; Qu, W. Precise molybdenite Re–Os and mica Ar–Ar dating of the Mesozoic Yaogangxian tungsten deposit, central Nanling district, South China. *Miner. Depos.* **2006**, *41*, 661–669. [CrossRef]

9. Li, S.T.; Wang, J.B.; Zhu, X.Y.; Wang, Y.L.; Han, Y.; Guo, N.N. Chronological characteristics of the Yaogangxian composite pluton in Hunan Province. *Geol. Explor.* **2011**, *47*, 143–150. (In Chinese)

10. Cao, J.Y.; Wu, Q.H.; Yang, X.Y.; Kong, H.; Li, H.; Xi, X.S.; Huang, Q.H.; Liu, B. Geochronology and Genesis of the Xitian W–Sn Polymetallic Deposit in Eastern Hunan Province, South China: Evidence from Zircon U–Pb and Muscovite Ar–Ar Dating, petrochemistry, and Wolframite Sr–Nd–Pb Isotopes. *Minerals* **2018**, *8*, 111. [CrossRef]

11. Dong, S.; Bi, X.; Hu, R.; Chen, Y. Petrogenesis of the Yaogangxian granites and implications for W mineralization, Hunan Province. *Acta Petrol. Sin.* **2014**, *30*, 2749–2765. (In Chinese)

12. Li, H.; Watanabe, K.; Yonezu, K. Geochemistry of A-type granites in the Huangshaping polymetallic deposit (South Hunan, China): Implications for granite evolution and associated mineralization. *J. Asian Earth Sci.* **2014**, *88*, 149–167. [CrossRef]

13. Zhao, K.; Jiang, S.; Jiang, Y.; Liu, D. SHRIMP U–Pb dating of the Furong unit of Qitangling granite from southeast Hunan province and their geological implications. *Acta Petrol. Sin.* **2006**, *22*, 2611–2616. (In Chinese)

14. Li, H.; Watanabe, K.; Yonezu, K. Zircon morphology, geochronology and trace element geochemistry of the granites from the Huangshaping polymetallic deposit, South China: Implications for the magmatic evolution and mineralization processes. *Ore Geol. Rev.* **2014**, *60*, 14–35. [CrossRef]

15. Chen, Y.; Li, H.; Sun, W.; Ireland, T.; Tian, X.; Hu, Y.; Yang, W.; Chen, C.; Xu, D. Generation of Late Mesozoic Qianlishan A2-type granite in Nanling Range, South China: Implications for Shizhuyuan W–Sn mineralization and tectonic evolution. *Lithos* **2016**, *266–267*, 435–452. [CrossRef]

16. Hu, X.; Gong, Y.; Pi, D.; Zhang, Z.; Zeng, G.; Xiong, S.; Yao, S. Jurassic magmatism related Pb–Zn–W–Mo polymetallic mineralization in the central Nanling Range, South China: Geochronologic, geochemical, and isotopic evidence from the Huangshaping deposit. *Ore Geol. Rev.* **2017**, *91*, 877–895. [CrossRef]

17. Xuan, Y.S.; Yuan, S.D.; Yuan, Y.B.; Mi, J.R. Zircon U–Pb age, geochemistry and petrogenesis of Jianfengling plutonin southern Hunan Province. *Miner. Depos.* **2014**, *33*, 1379–1390. (In Chinese)

18. Zhu, J.C.; Wang, R.C.; Lu, J.J.; Zhang, H.; Zhang, W.L.; Xie, L.; Zhang, R.Q. Fractionation, evolution, petrogenesis and mineralization of Laiziling Granite Pluton, Southern Hunan Province. *Geol. J. China Univ.* **2011**, *17*, 381–392. (In Chinese)

19. Xu, Q.D. Identification of the intrusive phases of the composite alkali-feldspathic granite in Xianghualing, Hunan. *Hunan Geol.* **1991**, *10*, 289–294. (In Chinese)

20. Wiedenbeck, M.; Alle, P.; Corfu, F.; Griffin, W.L.; Meier, M.; Ober, F.; Von Quadt, A.; Roddick, J.C.; Speigel, W. Three natural zircon standards for U–Th–Pb, Lu–Hf, trace-element and REE analyses. *Geostand. Geoanal. Res.* **1995**, *19*, 1–23. [CrossRef]

21. Liu, Y.; Gao, S.; Hu, Z.; Gao, C.; Zong, K.; Wang, D. Continental and oceanic crust recycling-induced melt-peridotite interactions in the Trans-North China Orogen: U–Pb Dating, Hf Isotopes and Trace Elements in Zircons from Mantle Xenoliths. *J. Petrol.* **2010**, *51*, 537–571. [CrossRef]

22. Liu, Y.; Hu, Z.; Gao, S.; Guenther, D.; Xu, J.; Gao, C.; Chen, H. In situ analysis of major and trace elements of anhydrous minerals by LA-ICP-MS without applying an internal standard. *Chem. Geol.* **2008**, *257*, 34–43. [CrossRef]

23. Andersen, T. Correction of common lead in U–Pb analyses that do not report 204Pb. *Chem. Geol.* **2002**, *192*, 59–79. [CrossRef]

24. Ludwig, K.R. *ISOPLOT 3.00: A Geochronological Toolkit for Microsoft Excel*; Berkeley Geochronology Center: Berkeley, CA, USA, 2003; p. 39.

25. Wu, F.; Yang, Y.; Xie, L.; Yang, J.; Xu, P. Hf isotopic compositions of the standard zircons and baddeleyites used in U–Pb geochronology. *Chem. Geol.* **2006**, *234*, 105–126. [CrossRef]

26. Geng, J.Z.; Li, H.K.; Zhang, J.; Zhou, H.Y.; Li, H.M. Zircon Hf isotope analysis by means of LA-MC-ICP-MS. *Geol. Bull. China* **2011**, *30*, 1508–1513. (In Chinese)

27. Machado, N.; Simonetti, A. U–Pb dating and Hf isotopic composition of Zircon by Laser-Ablation-MC-ICP-MS. In *Laser-Ablation-ICPMS in the Earth Sciences: Principles and Applications*; Sylvester, P., Ed.; Mineralogical Association of Canada: Québec, QC, Canada, 2001; Volume 29, pp. 121–146.

28. Chu, N.C.; Taylor, R.N.; Chavagnac, V.; Nesbitt, R.W.; Boella, R.M.; Milton, J.A.; German, C.R.; Bayon, G.; Burton, K. Hf isotope ratio analysis using multi-collector inductively coupled plasma mass spectrometry: An evaluation of isobaric interference corrections. *J. Anal. At. Spectrom.* **2002**, *17*, 1567–1574. [CrossRef]

29. Iizuka, T.; Hirata, T. Improvements of precision and accuracy in in situ Hf isotope microanalysis of zircon using the laser ablation-MC-ICPMS technique. *Chem. Geol.* **2005**, *220*, 121–137. [CrossRef]

30. Thirlwall, M.F.; Anczkiewicz, R. Multidynamic isotope ratio analysis using MC-ICP-MS and the causes of secular drift in Hf, Nd and Pb isotope ratios. *Int. J. Mass Spectrom.* **2004**, *235*, 59–81. [CrossRef]

31. Scherer, E.; Munker, C.; Mezger, K. Calibration of the lutetium-hafnium clock. *Science* **2001**, *293*, 683–687. [CrossRef] [PubMed]

32. BlichertToft, J.; Albarede, F. The Lu–Hf isotope geochemistry of chondrites and the evolution of the mantle-crust system. *Earth Planet. Sci. Lett.* **1997**, *148*, 243–258. [CrossRef]

33. Nowell, G.M.; Kempton, P.D.; Noble, S.R.; Fitton, J.G.; Saunders, A.D.; Mahoney, J.J.; Taylor, R.N. High precision Hf isotope measurements of MORB and OIB by thermal ionisation mass spectrometry: Insights into the depleted mantle. *Chem. Geol.* **1998**, *149*, 211–233. [CrossRef]

34. Griffin, W.L.; Pearson, N.J.; Belousova, E.; Jackson, S.E.; van Achterbergh, E.; O'Reilly, S.Y.; Shee, S.R. The Hf isotope composition of cratonic mantle: LAM-MC-ICPMS analysis of zircon megacrysts in kimberlites. *Geochim. Cosmochim. Acta* **2000**, *64*, 133–147. [CrossRef]

35. Hoskin, P.W.O.; Schaltegger, U. The composition of zircon and igneous and metamorphic petrogenesis. *Rev. Miner. Geochem.* **2003**, *53*, 27–62. [CrossRef]

36. Taylor, S.R.; McLennan, S.M. *Continental Crust: Its Composition and Evolution. An Examination of the Geochemical Record Preserved in Sedimentary Rocks*; Blackwell Science Inc.: Boston, MA, USA, 1985; p. 312.

37. Middlemost, E.A.K. Naming materials in the magma/igneous rock system. *Earth Sci. Rev.* **1994**, *37*, 215–224. [CrossRef]

38. Peccerillo, A.; Taylor, S. Geochemistry of Eocene calc–alkaline volcanic rocks from the Kastamonu area, northern Turkey. *Contrib. Mineral. Petrol.* **1976**, *58*, 63–81. [CrossRef]

39. Maniar, P.D.; Piccoli, P.M. Tectonic discrimination of granitoids. *Geol. Soc. Am. Bull.* **1989**, *101*, 635–643. [CrossRef]

40. Sun, S.S.; McDonough, W.F. Chemical and isotopic systematics of oceanic basalts: Implications for mantle compositions and processes. In *Magmatism in the Ocean Basins*; Saunders, A.D., Norry, M.J., Eds.; Geological Society of London Special Paper: London, UK, 1989; Volume 32, pp. 313–345.

41. Collins, W.J.; Beams, S.D.; White, A.J.R.; Chappell, B.W. Nature and origin of A-type granites with particular reference to SE Australia. *Contrib. Mineral. Petrol.* **1982**, *80*, 189–200. [CrossRef]

42. King, P.L.; White, A.J.R.; Chappell, B.W.; Allen, C.M. Characterization and origin of aluminous A-type granites from the Lachlan Fold Belt, Southeastern Australia. *J. Petrol.* **1997**, *38*, 371–391. [CrossRef]

43. Whalen, J.B.; Currie, K.L.; Chappell, B.W. A-type granites: Geochemical characteristics, discrimination and petrogenesis. *Contrib. Mineral. Petrol.* **1987**, *95*, 407–419. [CrossRef]

44. King, P.L.; Chappell, B.W.; Allen, C.M.; White, A.J.R. Are A-type granites the high temperature felsic granites? Evidence from fractionated granites of the Wangrah Suite. *Aust. J. Earth Sci.* **2001**, *48*, 501–514. [CrossRef]

45. Loiselle, M.C.; Wones, D.R. Characteristics and Origin of Anorogenic Granites. *Geochem. Soc. Am.* **1979**, *11*, 468.

46. Chappell, B.W. Aluminium saturation in I- and S-type granites and the characterization of fractionated haplogranites. *Lithos* **1999**, *46*, 535–551. [CrossRef]

47. Chappell, B.W.; White, A.J.R. Two contrasting granite types. *Pac. Geol.* **1974**, *8*, 173–174.

48. Chappell, B.W.; White, A. Two contrasting granite types: 25 years later. *Aust. J. Earth Sci.* **2001**, *48*, 489–499. [CrossRef]

49. Chappell, B.W.; Bryant, C.J.; Wyborn, D. Peraluminous I-type granites. *Lithos* **2012**, *153*, 142–153. [CrossRef]

50. Gao, P.; Zheng, Y.; Zhao, Z. Distinction between S-type and peraluminous I-type granites: Zircon versus whole-rock geochemistry. *Lithos* **2016**, *258–259*, 77–91. [CrossRef]

51. Wu, Q.; Cao, J.; Kong, H.; Shao, Y.; Li, H.; Xi, X.; Deng, X. Petrogenesis and tectonic setting of the early Mesozoic Xitian granitic pluton in the middle Qin-Hang Belt, South China: Constraints from zircon U–Pb ages and bulk-rock trace element and Sr–Nd–Pb isotopic compositions. *J. Asian Earth Sci.* **2016**, *128*, 130–148. [CrossRef]

52. Bonin, B. A-type granites and related rocks: Evolution of a concept, problems and prospects. *Lithos* **2007**, *97*, 1–29. [CrossRef]

53. Grebennikov, A.V. A-type granites and related rocks: Petrogenesis and classification. *Russ. Geol. Geophys.* **2014**, *55*, 1353–1366. [CrossRef]

54. Martin, R.F. A-type granites of crustal origin ultimately result from open-system fenitization-type reactions in an extensional environment. *Lithos* **2006**, *91*, 125–136. [CrossRef]

55. Pankhurst, M.J.; Schaefer, B.F.; Turner, S.P.; Argles, T.; Wade, C.E. The source of A-type magmas in two contrasting settings: U–Pb, Lu–Hf and Re–Os isotopic constraints. *Chem. Geol.* **2013**, *351*, 175–194. [CrossRef]

56. Frost, B.R.; Barnes, C.G.; Collins, W.J.; Arculus, R.J.; Ellis, D.J.; Frost, C.D. A geochemical classification for granitic rocks. *J. Petrol.* **2001**, *42*, 2033–2048. [CrossRef]

57. Frost, C.D.; Frost, B.R. On Ferroan (A-type) Granitoids: Their Compositional Variability and Modes of Origin. *J. Petrol.* **2011**, *52*, 39–53. [CrossRef]

58. Gilder, S.A.; Gill, J.; Coe, R.S.; Zhao, X.X.; Liu, Z.W.; Wang, G.X.; Yuan, K.R.; Liu, W.L.; Kuang, G.D.; Wu, H.R. Isotopic and paleomagnetic constraints on the Mesozoic tectonic evolution of south China. *J. Geophys. Res. Solid Earth* **1996**, *101*, 16137–16154. [CrossRef]

59. Jiang, S.Y.; Zhao, K.D.; Jiang, Y.H.; Dai, B.Z. Characteristics and genesis of Mesozoic A-type granites and associated mineral deposits in the southern Hunan and northern Guangxi provinces along the Shi-Hang belt, South China. *Geol. J. China Univ.* **2008**, *14*, 496–509. (In Chinese)

60. Cao, M.; Qin, K.; Li, G.; Evans, N.J.; McInnes, B.I.A.; Li, J.; Zhao, J. Oxidation state inherited from the magma source and implications for mineralization: Late Jurassic to Early Cretaceous granitoids, Central Lhasa subterrane, Tibet. *Miner. Depos.* **2018**, *53*, 299–309. [CrossRef]

61. Zhou, Y.; Liang, X.; Wu, S.; Cai, Y.; Liang, X.; Shao, T.; Wang, C.; Fu, J.; Jiang, Y. Isotopic geochemistry, zircon U–Pb ages and Hf isotopes of A-type granites from the Xitian W–Sn deposit, SE China: Constraints on petrogenesis and tectonic significance. *J. Asian Earth Sci.* **2015**, *105*, 122–139. [CrossRef]

62. Zhao, K.; Jiang, S.; Yang, S.; Dai, B.; Lu, J. Mineral chemistry, trace elements and Sr–Nd–Hf isotope geochemistry and petrogenesis of Cailing and Furong granites and mafic enclaves from the Qitianling batholith in the Shi-Hang zone, South China. *Gondwana Res.* **2012**, *22*, 310–324. [CrossRef]

63. Yuan, S.D. *Geochronology and Geochemistry of the Xianghualing Tin-Polymetallic Deposit, Hunan Province, China*; Institute of Geochemistry, Chinese Academy of Sciences: Guiyang, China, 2007. (In Chinese)

64. Boehnke, P.; Watson, E.B.; Trail, D.; Harrison, T.M.; Schmitt, A.K. Zircon saturation re-revisited. *Chem. Geol.* **2013**, *351*, 324–334. [CrossRef]

65. Ferry, J.M.; Watson, E.B. New thermodynamic models and revised calibrations for the Ti-in-zircon and Zr-in-rutile thermometers. *Contrib. Mineral. Petrol.* **2007**, *154*, 429–437. [CrossRef]

66. Liu, H.; Xu, Y.; He, B. Implications from zircon-saturation temperatures and lithological assemblages for Early Permian thermal anomaly in northwest China. *Lithos* **2013**, *182*, 125–133. [CrossRef]

67. Miller, C.F.; McDowell, S.M.; Mapes, R.W. Hot and cold granites? Implications of zircon saturation temperatures and preservation of inheritance. *Geology* **2003**, *31*, 529–532. [CrossRef]

68. Watson, E.B.; Harrison, T.M. Zircon saturation revisited: Temperature and composition effects in a variety of crustal magma types. *Earth Planet. Sci. Lett.* **1983**, *64*, 295–304. [CrossRef]

69. Watson, E.B.; Harrison, T.M. Zircon thermometer reveals minimum melting conditions on earliest Earth. *Science* **2005**, *308*, 841–844. [CrossRef] [PubMed]

70. Barth, A.P.; Wooden, J.L. Coupled elemental and isotopic analyses of polygenetic zircons from granitic rocks by ion microprobe, with implications for melt evolution and the sources of granitic magmas. *Chem. Geol.* **2010**, *277*, 149–159. [CrossRef]

71. Brounce, M.; Kelley, K.A.; Cottrell, E.; Reagan, M.K. Temporal evolution of mantle wedge oxygen fugacity during subduction initiation. *Geology* **2015**, *43*, 775–778. [CrossRef]

72. Lee, C.A.; Luffi, P.; Chin, E.J.; Bouchet, R.; Dasgupta, R.; Morton, D.M.; Le Roux, V.; Yin, Q.; Jin, D. Copper systematics in Arc magmas and implications for crust-mantle differentiation. *Science* **2012**, *336*, 64–68. [CrossRef] [PubMed]

73. Lee, C.; Leeman, W.P.; Canil, D.; Li, Z. Similar V/Sc systematics in MORB and arc basalts: Implications for the oxygen fugacities of their mantle source regions. *J. Petrol.* **2005**, *46*, 2313–2336.

74. Qiu, J.; Yu, X.; Santosh, M.; Zhang, D.; Chen, S.; Li, P. Geochronology and magmatic oxygen fugacity of the Tongcun molybdenum deposit, northwest Zhejiang, SE China. *Miner. Depos.* **2013**, *48*, 545–556. [CrossRef]

75. Sun, W.; Huang, R.; Li, H.; Hu, Y.; Zhang, C.; Sun, S.; Zhang, L.; Ding, X.; Li, C.; Zartman, R.E.; et al. Porphyry deposits and oxidized magmas. *Ore Geol. Rev.* **2015**, *65*, 97–131. [CrossRef]

76. Sun, W.; Liang, H.; Ling, M.; Zhan, M.; Ding, X.; Zhang, H.; Yang, X.; Li, Y.; Ireland, T.R.; Wei, Q.; et al. The link between reduced porphyry copper deposits and oxidized magmas. *Geochim. Cosmochim. Acta* **2013**, *103*, 263–275. [CrossRef]

77. Xiao, B.; Qin, K.; Li, G.; Li, J.; Xia, D.; Chen, L.; Zhao, J. Highly oxidized magma and fluid evolution of Miocene Qulong Giant Porphyry Cu-Mo deposit, Southern Tibet, China. *Resour. Geol.* **2012**, *62*, 4–18. [CrossRef]

78. Gao, X.-Q.; He, W.-Y.; Gao, X.; Bao, X.-S.; Yang, Z. Constraints of magmatic oxidation state on mineralization in the Beiya alkali-rich porphyry gold deposit, western Yunnan, China. *Solid Earth Sci.* **2017**, *2*, 65–78. [CrossRef]

79. Yang, Z.; Yang, L.; He, W.; Gao, X.; Liu, X.; Bao, X.; Lu, Y. Control of magmatic oxidation state in intracontinental porphyry mineralization: A case from Cu (Mo–Au) deposits in the Jinshajiang-Red River metallogenic belt, SW China. *Ore Geol. Rev.* **2017**, *90*, 827–846.

80. Trail, D.; Watson, E.B.; Tailby, N.D. Ce and Eu anomalies in zircon as proxies for the oxidation state of magmas. *Geochim. Cosmochim. Acta* **2012**, *97*, 70–87. [CrossRef]

81. Trail, D.; Watson, E.B.; Tailby, N.D. The oxidation state of Hadean magmas and implications for early Earth's atmosphere. *Nature* **2011**, *480*, 79–238. [CrossRef] [PubMed]

82. Sun, Z.L. Geochronology and oxygen fugacity of Mesozoic granites in Nanling area of South China. *J. Earth Sci. Environ.* **2014**, *36*, 141–151. (In Chinese)

83. Burnham, A.D.; Berry, A.J. An experimental study of trace element partitioning between zircon and melt as a function of oxygen fugacity. *Geochim. Cosmochim. Acta* **2012**, *95*, 196–212. [CrossRef]

84. Ballard, J.R.; Palin, J.M.; Campbell, I.H. Relative oxidation states of magmas inferred from Ce(IV)/Ce(III) in zircon: Application to porphyry copper deposits of northern Chile. *Contrib. Mineral. Petrol.* **2002**, *144*, 347–364. [CrossRef]

85. Eugster, H.P.; Wones, D.R. Stability relations of the ferruginous Biotite, Annite. *J. Petrol.* **1962**, *3*, 82–89. [CrossRef]

86. Skjerlie, K.P.; Johnston, A.D. Fluid-Absent Melting Behavior of an F-Rich Tonalitic Gneiss at Mid-Crustal Pressures: Implications for the Generation of Anorogenic Granites. *J. Petrol.* **1993**, *34*, 785–815. [CrossRef]

87. Rutanen, H.; Andersson, U.B.; Vaisanen, M.; Johansson, A.; Frojdo, S.; Lahaye, Y.; Eklund, O. 1.8 Ga magmatism in southern Finland: Strongly enriched mantle and juvenile crustal sources in a post-collisional setting. *Int. Geol. Rev.* **2011**, *53*, 1622–1683. [CrossRef]

88. Villaseca, C.; Orejana, D.; Belousova, E.A. Recycled metaigneous crustal sources for S- and I-type Variscan granitoids from the Spanish Central System batholith: Constraints from Hf isotope zircon composition. *Lithos* **2012**, *153*, 84–93. [CrossRef]

89. Yang, J.H.; Wu, F.Y.; Chung, S.L.; Wilde, S.A.; Chu, M.F. A hybrid origin for the Qianshan, A-type granite, northeast China: Geochemical and Sr–Nd–Hf isotopic evidence. *Lithos* **2006**, *89*, 89–106. [CrossRef]

90. Zhang, Y.; Yang, J.; Chen, J.; Wang, H.; Xiang, Y. Petrogenesis of Jurassic tungsten-bearing granites in the Nanling Range, South China: Evidence from whole-rock geochemistry and zircon U–Pb and Hf–O isotopes. *Lithos* **2017**, *278–281*, 166–180. [CrossRef]

91. Cai, Y. *The Study on Dengfuxian Granite and Its Mineralization in Hunan Province*; Nanjing University: Nanjing, China, 2013. (In Chinese)

92. Guo, C.; Chen, Y.; Zeng, Z.; Lou, F. Petrogenesis of the Xihuashan granites in southeastern China: Constraints from geochemistry and in-situ analyses of zircon U–Pb–Hf–O isotopes. *Lithos* **2012**, *148*, 209–227. [CrossRef]

93. Guo, C.; Zeng, L.; Li, Q.; Fu, J.; Ding, T. Hybrid genesis of Jurassic fayalite-bearing felsic subvolcanic rocks in South China: Inspired by petrography, geochronology, and Sr–Nd–O–Hf isotopes. *Lithos* **2016**, *264*, 175–188. [CrossRef]

94. Gu, S.Y.; Hua, R.M.; Qi, H.W. Zircon LA-ICP-MS U–Pb dating and Sr-Nd isotope study of the Guposhan granite complex, Guangxi, China. *Chin. J. Geochem.* **2006**, *26*, 290–300. [CrossRef]

95. Eby, G.N. Chemical subdivision of the A-type granitoids: Petrogenetic and tectonic implications. *Geology* **1992**, *20*, 641–644. [CrossRef]

96. Pearce, J.A.; Harris, N.B.W.; Tindle, A.G. Trace-element discrimination diagrams for the tectonic interpretation of granitic-rocks. *J. Petrol.* **1984**, *25*, 956–983. [CrossRef]

97. Chen, C.; Lee, C.; Shinjo, R. Was there Jurassic paleo-Pacific subduction in South China? Constraints from (40)Ar/(39)Ar dating, elemental and Sr–Nd–Pb isotopic geochemistry of the Mesozoic basalts. *Lithos* **2008**, *106*, 83–92. [CrossRef]

98. Honza, E.; Fujioka, K. Formation of arcs and backarc basins inferred from the tectonic evolution of Southeast Asia since the Late Cretaceous. *Tectonophysics* **2004**, *384*, 23–53. [CrossRef]

99. Jiang, Y.; Jiang, S.; Dai, B.; Liao, S.; Zhao, K.; Ling, H. Middle to late Jurassic felsic and mafic magmatism in southern Hunan province, southeast China: Implications for a continental arc to rifting. *Lithos* **2009**, *107*, 185–204. [CrossRef]

100. Jiang, Y.; Jiang, S.; Zhao, K.; Ling, H. Petrogenesis of Late Jurassic Qianlishan granites and mafic dykes, Southeast China: Implications for a back-arc extension setting. *Geol. Mag.* **2006**, *143*, 457–474. [CrossRef]

101. Li, Z.; Li, X. Formation of the 1300-km-wide intracontinental orogen and postorogenic magmatic province in Mesozoic South China: A flat-slab subduction model. *Geology* **2007**, *35*, 179–182. [CrossRef]

102. Qiu, Z.; Li, S.; Yan, Q.; Wang, H.; Wei, X.; Li, P.; Wang, L.; Bu, A. Late Jurassic Sn metallogeny in eastern Guangdong, SE China coast: Evidence from geochronology, geochemistry and Sr–Nd–Hf–S isotopes of the Dadaoshan Sn deposit. *Ore Geol. Rev.* **2017**, *83*, 63–83. [CrossRef]

103. Sun, W.; Ding, X.; Hu, Y.; Zartman, R.E.; Arculus, R.J.; Kamenetsky, V.S.; Chen, M. The fate of subducted oceanic crust: A mineral segregation model. *Int. Geol. Rev.* **2011**, *53*, 879–893. [CrossRef]

104. Sun, W.; Ling, M.; Yang, X.; Fan, W.; Ding, X.; Liang, H. Ridge subduction and porphyry copper-gold mineralization: An overview. *Sci. China Earth Sci.* **2010**, *53*, 475–484. [CrossRef]

105. Xie, G.Q.; Hu, R.Z.; Zhao, J.H.; Jiang, G.H. Mantle plume and the relationship between it and Mesozoic large-scale metallogenesis in southeastern China: A preliminary discussion. *Geotecton. Metallog.* **2001**, *25*, 179–186. (In Chinese)

106. Zhao, W.W.; Zhou, M.; Li, Y.H.M.; Zhao, Z.; Gao, J. Genetic types, mineralization styles, and geodynamic settings of Mesozoic tungsten deposits in South China. *J. Asian Earth Sci.* **2017**, *137*, 109–140. [CrossRef]

107. Zhou, X.M.; Li, W.X. Origin of Late Mesozoic igneous rocks in Southeastern China: Implications for lithosphere subduction and underplating of mafic magmas. *Tectonophysics* **2000**, *326*, 269–287. [CrossRef]

108. Fan, W.M.; Wang, Y.; Guo, F.; Peng, T.P. Mezosic mafic magmatism in Hunan-Jiangxi provinces and the lithospheric extension. *Earth Sci. Front.* **2003**, *10*, 159–169. (In Chinese)

109. Wang, Y.J.; Liao, C.L.; Fan, W.M.; Peng, T. Early Mesozoic OIB-type alkaline basalt in central Jiangxi province and its tectonic implications. *Geochimica* **2004**, *33*, 109–117.